Article

Satellite-Derived Topography and Morphological Evolution around Authie Macrotidal Estuary (France)

Philippe Bagot [1],* , Nicolas Huybrechts [2] and Philippe Sergent [2]

1. Cerema, Technopôle Brest-Iroise, 155 Rue Pierre Bouguer, BP5, 29280 Plouzané, France
2. Cerema, HA Research Team, 134 Rue de Beauvais, 60200 Compiegne, France;
   nicolas.huybrechts@cerema.fr (N.H.); Philippe.Sergent@cerema.fr (P.S.)
* Correspondence: philippe.bagot@cerema.fr

Abstract: The wide spatial and temporal coverage of remotely sensing images is an essential asset to analyze the morphological behaviour of fast-changing coastal environments such as estuarine systems. This paper investigates the reliability of intertidal topography mapping around the Authie Bay, a macrotidal estuarine system located on the northern coast of France. A Satellite-Derived Topography technique is developed by relating the green band reflectance of Sentinel-2 images to rapid variations in topography. This method is well suited to small sedimentary structures of the coastal zone with a 0.30 to 0.35 m height accuracy of the constructed Digital Elevation Model (DEM). For the more complex estuarine configuration, the waterline method was applied and resulted in the construction of DEMs with a height accuracy of 0.35 to 0.38 m. Video animations and records of Authie meander positions along transects are created from Sentinel-2 and Landsat satellite archives (1984–2020). These materials allow to highlight a sedimentation phase at the east side of the spit since 2015. It constrains the main channel towards the eastern bank, thus promoting coastal erosion. The monitoring of a severe erosion phase throughout 2019 shows a 130 m retreat of the coastline. Topographic map differentiation led to the detection of a sedimentation anomaly upstream of the bay, probably linked to this erosion event.

Keywords: coastal monitoring; satellite derived topography; sandspit; morphological changes; remote sensing; waterline method

1. Introduction

Exposed to natural processes and human activities, estuarine systems are subject to morphological changes. In particular, many estuaries show an overall trend to sedimentary infilling since the beginning of the Holocene epoch [1,2]. A mutual interaction takes place between the morphology and the current patterns. Thus, the deposition of sediment from the sea changes the morphology of the estuary, which in turn modifies the tidal currents and the sediment import, leading to a morphodynamic feedback [3,4]. Since sea level rise is expected to hamper estuary infilling, the morphological response of estuaries is uncertain and may depend on the size of the estuary [5]. In the context of global warming, storm-surge effects are made worse by sea-level rise and pose a threat to populations. Hence, a long-term sustainable management requires a better understanding of the morphological changes in estuaries and coastal environments. This implies an accurate bathymetric information with a high temporal frequency in dynamic areas. Traditional methods consist in field surveys with ship based multi-beam echosounder or airborne Lidar systems, which provide high accuracy measurements within a few centimeters [6]. However the cost of and time spent on these approaches impede large scale repetitive surveys. Since the last decade, remote sensing techniques, with increasing accuracy, are emerging as a complementary and low-cost alternative to conventional methods.

The interest of satellite imagery is twofold: the extensive spatial and temporal coverage. Firstly, spatial coverage allows a broad-scale bathymetry and topography of the

area. Several remote sensing techniques for seafloor mapping of nearshore and intertidal areas have been used in the last years (see the review in [7]). Satellite-Derived Bathymetry (SDB) is based on the spectral information from the sunlight reflected from the seafloor and inversion algorithms to calculate water column depth [8–10]. Although SDB is the most common technique used for shallow waters, its application is constrained by water transparency conditions. In particular, in highly dynamic areas, like estuarine systems, bathymetric inversion in turbid water produces false shoals signals [11,12]. Another approach is to construct DEMs of the intertidal zone from Satellite-Derived Topography (SDT) techniques. The waterline method, which relies on a set of heightened waterlines from multiple satellite images, is a well-established SDT technique for retrieving intertidal topography [13–16]. The second interest of satellite imagery is its wide temporal coverage, which allows the monitoring of fast-changing areas. Dynamics of the shoreline position have been investigated in [17,18] using multi-temporal satellite images, leading to the identification of shoreline areas with high erosional activity and zones facing rapid shoreline progression. In addition, historical archives of remote sensing open source data are useful to analyze the morphological behaviour of coastal inlets. In [19], a set of 79 SPOT images from 1986 to 2012 were used to build a SPOT-derived bathymetry allowing the monitoring of evolutionary changes in sedimentary structures.

This study takes advantage of satellite imagery to improve our knowledge of the hydrodynamic functioning of the Authie Bay, a rapidly evolving macrotidal estuarine system located on the northern coast of France. The objective of this paper is both to evaluate the height accuracy of satellite mapping techniques over this area and to analyze the complex processes at work in the bay using remote sensing archives. The study area consists of two sites, the Berck shoreline close to the estuary and the Authie Bay itself. In this highly turbid environment, SDT methods are preferred in order to overcome the limited performance of SDB techniques due to poor water transparency conditions. A SDT method based on the green band reflectance of a Sentinel-2 satellite image is developed for the mapping of the Berck shoreline site, while the waterline method is used to map the Authie Bay. Long-term morphological changes are monitored from a collection of Landsat and Sentinel-2 satellite images over the period 1984 to 2020.

Details of the resources and methods are provided in Section 2. The SDT maps made on the Berck shoreline and Authie Bay sites, the morphological evolution observed on timelapses, and the meander monitoring of the Authie River are presented in Section 3. Finally, in Section 4, the relevance of SDT models is discussed, followed by an analysis of the morphological changes and the sedimentation anomaly detected upstream of the estuary.

2. Materials and Methods

2.1. Study Sites

For this study, two areas were selected, the Authie estuary and a portion of the shore near Berck city. Figure 1a indicates the location of both study sites. Authie Bay is the main site while the Berck shoreline is a reference area experiencing the same environmental conditions but without the complex hydro-sedimentary processes of the bay. The Authie Bay (17 km^2) is one of the three estuaries which mark out the Picardy maritime plain, the other two being the Somme Bay (70 km^2) and the Canche estuary (10 km^2). The 98 km long coastal river originates from a limestone plateau catchment of 989 km^2. The Authie river inflow is small with a mean annual discharge of 10 m^3/s, and due to the nature of the bedrock geology, it brings little sediment to the coastal zone [20,21]. With a mean spring and neap tide ranges of 8.5 m and 4.9 m at its mouth, respectively, the Authie Bay is a macrotidal system, influenced by both tides and waves [4]. These tidal ranges decrease to 4 m and 1.8 m upstream of the estuary while the influence of spring tides extends up to 16 km inland [22]. Strong tidal currents that can reach 1.5 m/s are generated at the estuary mouth and adjacent coastal zone during spring tides [23]. Winter storms can lead to water level rises above 1 m at the entrance of the estuary [24].

The Authie Bay is a sand-filled estuary with a typical geomorphological structure. The west provenance of waves resulted in a northward littoral drift, leading to the northward progradation of the south coast at a rate of 6.1 m/yr between 2005–2012 and the formation of an extensive intertidal sand platform [21,25]. Over the last three centuries, the sand platform extended northwards [23], confining the Authie river towards the opposite shore, which led to the formation of a narrow deep inlet channel at the northern side (Figure 1b). As a result of the spit accretion, sediment infilling and river meandering, the thick dune barrier of the northern coastline is subject to erosion, such as the Bois des Sapins area. The reworked sediments contribute to the sand filling of the inner estuary mainly fed by the sediment import from the sea [26]. This sand transport resulted in the formation of a secondary spit structure, the Bec du Perroquet area, prograding southwards [21]. The spit platform partially protects the estuary by dissipating the energy of storm swells. In this sheltered environment, tidal flats and salt marshes are present along a meandering Authie channel. Landscaping has been carried out over the past few centuries, resulting in the reclamation of large portions of the inner estuary [24,25]. The land behind Authie Bay is particularly exposed to the risk of marine submersion due to the erosion of the dune cordon which, in particular, suffered a severe erosion event in 2019.
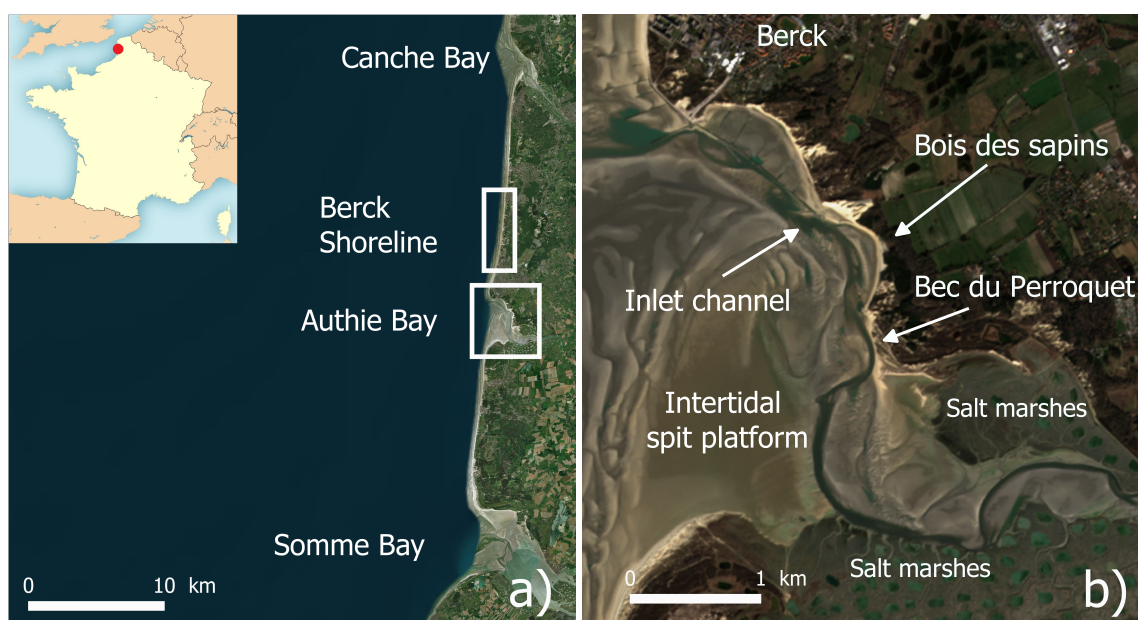

Figure 1. Location of the study sites on the northern coast of France. (**a**) The white rectangle box represents a portion of the north coast along Berck city between the bays of Authie and Canche, while the white square box indicates the Authie estuary. (**b**) Zoom of the Authie Bay. Bois des Sapins and Bec du Perroquet labels refer to specific areas that have experienced erosion in recent years. Source: Sentinel-2 RGB composite imagery.

2.2. Survey Data

For the shoreline in the north of Berck, topographic data were collected by drone flights in October 2018 and 2019. The DEMs are constructed via the measurement of ground points for the georeferencing. The accuracy of the DEMs expected is 5–10 cm (horizontal or vertical) outside the vegetated area. Inside the Authie estuary, two measurement campaigns took place in February and October 2019. The dataset of each survey merges bathymetric data collected with a vessel and topographic data collected with a GPS. The accuracy is 5 cm for the bathymetry and 2 cm for the topography.

2.3. Imagery

In order to give insights of the estuarine dynamics in the last decades, a dense collection of remote sensing images is required. For this, Landsat-5, Landsat-7 and Landsat-8 images were selected from April 1984 to September 2020, enriched with Sentinel-2A and

2B scenes from August 2015 to September 2020. Remote sensing images were downloaded from the Sentinel hub data browser [27] which provides products with geometric correction, geo-referred to as WGS 84.

The temporal resolution of each Landsat is 16 days. Different sensors on board: Thematic Mapper (Landsat-5), Enhanced Thematic Mapper (Landsat-7) and Operational Land Imager (Landsat-8) allow a 30 m spatial resolution for the spectral bands of interest. Sentinel 2A and 2B twin polar orbiting satellites have 5 days revisit time, and the Multi Spectral Instrument provides a spatial resolution of 10 m. Figure 2 summarizes the imagery data timeline. False color composite images were preferred (i.e., NIR, red and green bands). Light in the near infrared band has a very low transmittance in sea water. Therefore, water appearing darker is better distinguished from sand. This is especially useful to not reject scenes with a cloudy veil, thus allowing a total number of 413 images over this period. The average number of selected Landsat images was around seven per year between 1985 and 2020, while this number has been above 30 per year since 2015 for Sentinel-2.
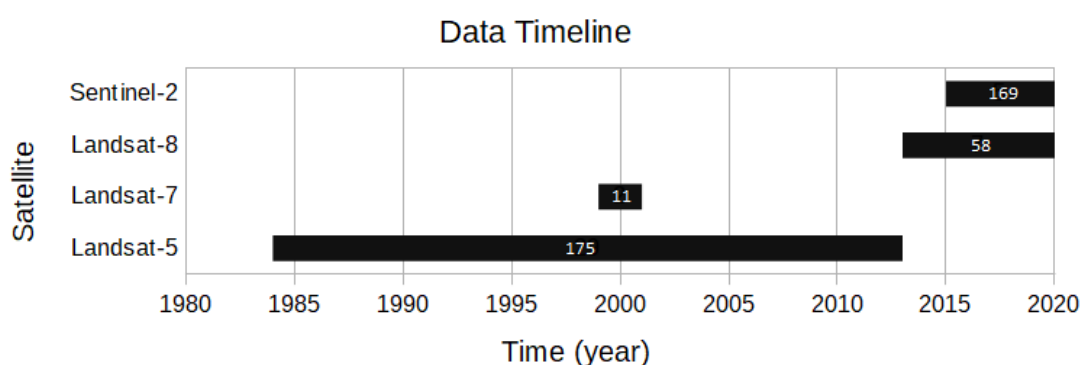

Figure 2. Temporal coverage of satellite imagery dataset used for timelapses of the Authie Bay and stability chronicles of the river. White labels refer to the number of selected images.

Regarding SDT based on the waterline method, Table 1 provides the wavelength ranges of Sentinel imagery. Sentinel-2 images that met the following conditions were selected (Table 2): (i) 0% cloud cover over the study area; (ii) acquisition date as close as possible to that of bathymetric and topographic surveys to ensure a low drift of sandbanks in dynamic areas over this period, i.e., no more than two months of time lag; and (iii) scenes with different tidal stages ensuring spaced waterlines.

Table 1. Sentinel-2 sensor specifications relevant to this study.

Band Number	Band Name	Central Wavelength (nm)	Band Width (nm)	Spatial Resolution (m)
2	B02-Blue	490	65	10
3	B03-Green	560	35	10
4	B04-Red	665	30	10
8	B08-NIR	842	115	10
11	B11-SWIR	1610	90	20

Table 2. Remote sensing images at different tidal stages, used in SDT methods. The time lag refers to the time difference between the acquisition dates of satellite images and ground in situ measurements.

Study Site	Acquisition Date	Time Lag in Weeks	Mission	Tide Level
Berck shoreline	26 September 2018	−3	Sentinel-2	High
	16 October 2018	0	Sentinel-2	Low
Berck shoreline	1 September 2019	−3	Sentinel-2	High
	21 September 2019	0	Sentinel-2	Low
Authie Bay	19 January 2019	−4	Sentinel-2	Intermediate
	21 January 2019	−4	Sentinel-2	High
	15 February 2019	0	Sentinel-2	Low
	23 February 2019	1	Sentinel-2	Low
	25 February 2019	1	Sentinel-2	Low
	1 April 2019	6	Sentinel-2	Intermediate Low
	6 April 2019	7	Landsat-8	Intermediate High
	21 April 2019	9	Sentinel-2	Intermediate
Authie Bay	1 September 2019	−5	Sentinel-2	Intermediate High
	8 September 2019	−4	Sentinel-2	Low
	21 September 2019	−2	Sentinel-2	Low
	28 October 2019	4	Sentinel-2	High
	10 November 2019	5	Sentinel-2	Intermediate
	17 November 2019	6	Sentinel-2	Low
	30 November 2019	8	Sentinel-2	Intermediate Low

2.4. Satellite Derived Topography

2.4.1. Berck Shoreline Site

SDB is based on reflectance information from a high tide remote sensing image but is constrained by the turbidity of the water column. The question of whether the reflectance of a low tide image can be used to construct a DEM needs to be further explored. Figure 3 shows the joint evolution of the topography and reflectance of the green band B03, along a transect of the intertidal zone. It appears that height information is carried by the reflectance since rapid variations in reflectance are correlated with those of the topography.

In signal theory, Amplitude Modulation is a modulation over time in which the amplitude of the carrier wave is altered in accordance with the instantaneous amplitude of the modulating signal. In this study, it is assumed that the observed topographic signal z_{obs} can be modelized by z_{model}, a combination of a slowly varying signal over space (the modulating signal) z_{slow} derived from the beach profile and a fast varying signal over space (the carrier wave) z_{B03} related to the reflectance of the green band ρ_{B03}. For the sake of simplicity, the two topographic signals are added instead of multiplied each other for each pair of geographical coordinates (x, y):

$$z_{model}(x, y) = z_{slow}(x, y) + z_{B03}(x, y) \tag{1}$$

The DEM corresponding to the slowly varying signal z_{slow} is constructed by interpolating the low and high tide waterlines whose heights are taken from the observed data and adjusted so that the sum of the slow and rapidly varying signals corresponds to the observed DEM value. In practice, this means that the observed height is assigned to the low tide waterline for which the reflectance is minimal (Figure 3c), and an observed height reduced by an arbitrary offset (e.g., two meters) is assigned to the high tide waterline for which the reflectance is maximal along the beach. By differentiating DEMs, i.e., corresponding to $z_{obs}(x, y) - z_{slow}(x, y)$, the rapidly varying topographic signal is then searched as a linear relationship of the reflectance: $z_{B03}(x, y) = a * \rho_{B03}(x, y) + b$. The best fit is obtained by varying the offset imposed on the height of the high tide waterline.
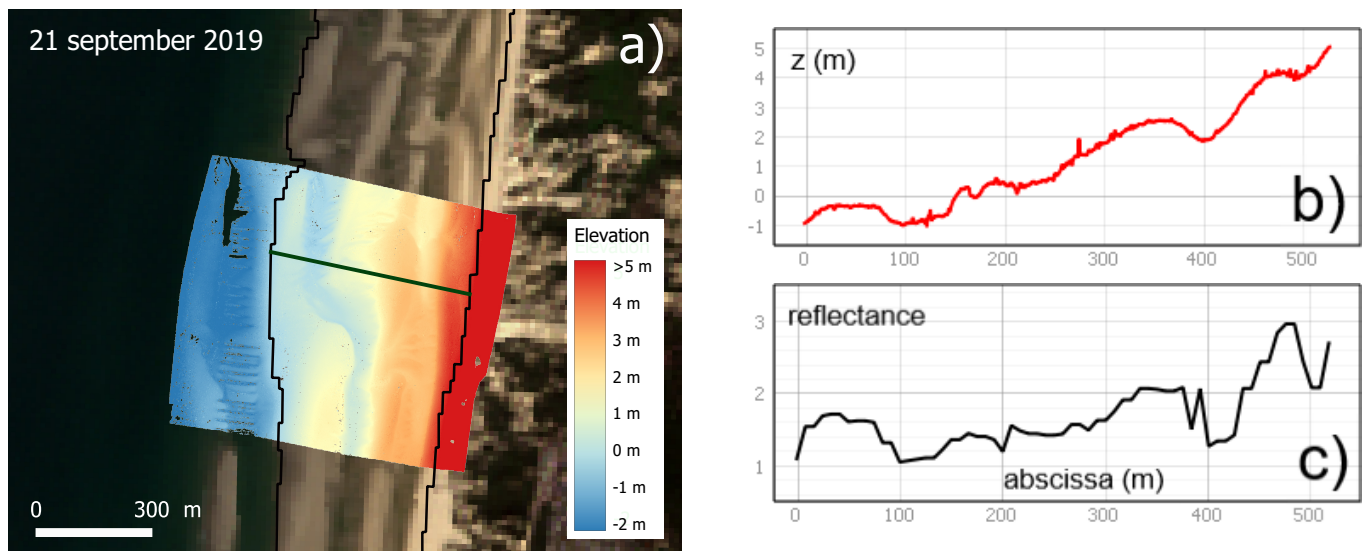
Figure 3. (**a**) DEM constructed from the observations, superimposed on a Sentinel-2 image of the Berck shoreline site. The intertidal zone is delimited by the black lines and the chosen transect is for the comparison of the elevation profile of the beach from west to east (**b**) with the dimensionless B03 reflectance of the multi-spectral Sentinel-2 image (**c**).

2.4.2. Authie Bay Site

While the method developed above is well suited to homogeneous areas such as the Berck shoreline, it is not for heterogeneous sites such as the Authie Bay. The variable size of the sedimentary structures and the spit platform prevent the definition of a slowly varying signal and implies changes in concavity. For estuarine configuration, the waterline method is preferred since it is an effective remote sensing technique for constructing DEM for large-scale tidal flat [28,29].

The method consists in detecting the land-sea boundary from satellite images, using edge detection algorithms or by visual investigation [30], under a wide range of tidal conditions. In the literature, heights are assigned to these waterlines using water level information provided either by sea level records from nearby tide gauges, a hydrodynamic model, or in situ measured data. From the set of heightened waterlines, a gridded DEM of the intertidal zone can be interpolated. In practice, the difficulty is to collect sufficient remote sensing images despite local weather conditions, in environments with high morphological changes such as estuarine systems.

In this study, the time span of the Sentinel-2 image acquisition dates is limited to three months (Table 2), so that the morphological changes are not too pronounced. Due to the moderate size of the Authie Bay, manual digitization of the waterlines is not time consuming. Field surveys conducted on Authie Bay in February and October 2019 are used to assign a height to these waterlines. Waterlines calibrated then allow the construction of a DEM by triangulation in order to follow the morphological evolution of the bay during the year 2019.

2.5. Timelapses

From the collection of 413 Landsat and Sentinel-2 satellite images, scenes without cloud cover are extracted and assembled into video animations that provide information on the morphodynamics of the bay from 1984 to 2020. The different animations depend on the nature of the information sought: the link between the Somme, Authie and Canche bays (wide field timelapse); the evolution of sedimentary structures (timelapse centered on the bay with low tide images) and the evolution of the Authie tidal basin over time (timelapse centered on the bay with intermediate tide images).

2.6. Monitoring of the Authie Meanders

Timelapses give a first qualitative information. Since the images are geo-referred, it is thus possible to infer quantitative information by recording the position of the Authie flow channel on transects of interest, over a long period of time. Two transects are positioned downstream of the bay to monitor areas that have eroded in recent years: Bois des Sapins (transect A) and Bec du Perroquet (transect B). Transects C and D, positioned in the inner bay, are useful to compare the evolution of the Authie flow channel between upstream and downstream of the bay. The maximum error on the surveyed positions is estimated at two pixels, i.e., 60 m for the Landsat images and 20 m for the Sentinel-2 images, which is sufficient for the monitoring of the Authie flow channel within the one kilometer wide tidal basin, between the spit platform and the shoreline.

3. Results

3.1. Berck Shoreline Site

Figure 4 displays the different steps in the construction of the topographic signal corresponding to the low tide Sentinel-2 image in September 2019. The first step is to build the slow varying topographic signal z_{slow} by interpolating the waterlines of the intertidal zone. Since the reflectance ρ_{B03} is minimal on the low tide waterline, no offset is needed, and the height assigned to the low tide (LT) waterline is the height from the observations $z_{obs}(LT) = -1.1$ m. On the other hand, regarding the high tide (HT) waterline, the assigned height is the observed value $z_{obs}(HT) = 4.8$ m minus an arbitrary offset of 2.20 m to take into account the maximum reflectance of the green band on this line. The result of the interpolation (Figure 4a) is a smooth topographic signal of the intertidal zone. The second step is to construct the fast varying signal z_{B03} by fitting the difference between the observed data DEM and the smooth signal DEM to the green band reflectance ρ_{B03}. The resulting linear fit is

$$z_{B03}(2019) = 1.210 * \rho_{B03} - 1.262 \equiv z_{obs} - z_{slow} \tag{2}$$

The rapidly varying signal shown in Figure 4b discriminates well against the sedimentary bars, which are about one meter high. The final step is to modulate the height of these dunes according to their relative position on the beach, i.e., by adding the two previously calculated signals to construct the final topographic signal shown in Figure 4c. The agreement with the measured values (Figure 4d) is quantified by a coefficient of determination R^2 equal to 0.950 and a root mean squared error of 0.345 m. The best value of the 2.20 m offset was obtained after successive iterations of this whole process. Figure 4e shows an example of the elevation profile along a transect for the observed values and the reconstructed signal. This method is also applied to a low-tide Sentinel-2 image from October 2018, for which in situ measurements are available. The rapidly varying signal is constructed from the fit:

$$z_{B03}(2018) = 0.947 * \rho_{B03} - 1.113 \tag{3}$$

The reconstructed topographic signal of the intertidal zone (Figure 5a) is in agreement with the observed data: R^2 is equal to 0.965, and the root mean squared error is 0.300 m, for an offset value of 1 m. Differentiation of the DEMs allows to monitor the elevation changes over the period 2018 to 2019. The resulting map (Figure 5c) is thus the mark of the longshore drift over a one-year period.
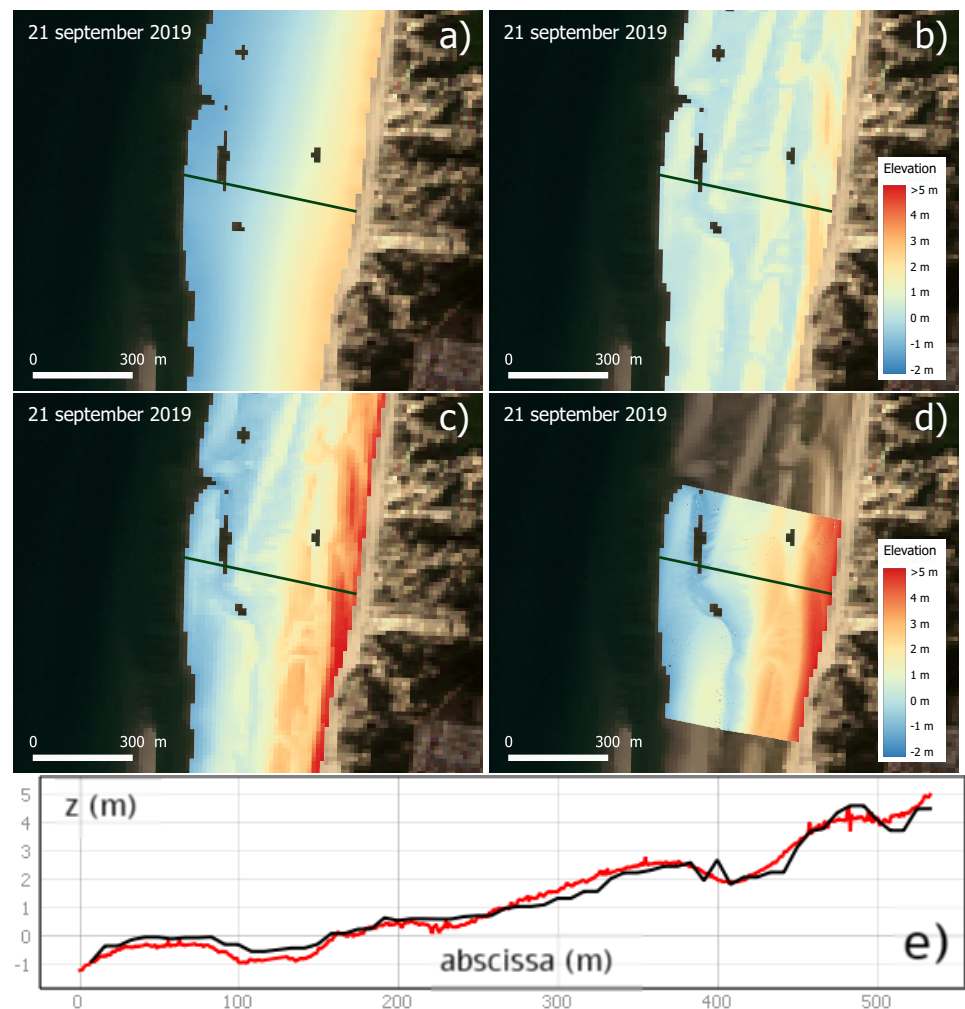
Figure 4. (**a**) Slowly varying signal DEM (z_{slow}), superimposed on a Sentinel-2 image of the Berck shoreline site. (**b**) Fast varying signal DEM (z_{B03}) related to the green band reflectance. (**c**) DEM constructed from the elevation model $z_{model} = z_{slow} + z_{B03}$. (**d**) Observed data DEM (z_{obs}). (**e**) Elevation profiles along the chosen transect according to z_{model} (black), compared to observed data z_{obs} (red).

3.2. Authie Bay Site

3.2.1. Satellite Derived Topography

The method developed for the Berck shoreline cannot be applied to the Authie Bay because of the changes in slope which cannot be simply reproduced by the reflectance variations of the green band. On the other hand, the topographic signal can be constructed by the conventional waterline method, at the risk of losing information if the study area evolves rapidly. Due to the rapid dynamics of the bay, only remotely sensed images that are less than two months apart from the date of the field survey are considered in this study (Table 2). Thus, for the February 2019 measurement survey, 7 Sentinel-2 images and one Landsat-8 image were selected for their various tidal levels. The heights from the observations were assigned to the manually digitized waterlines (Figure 6).
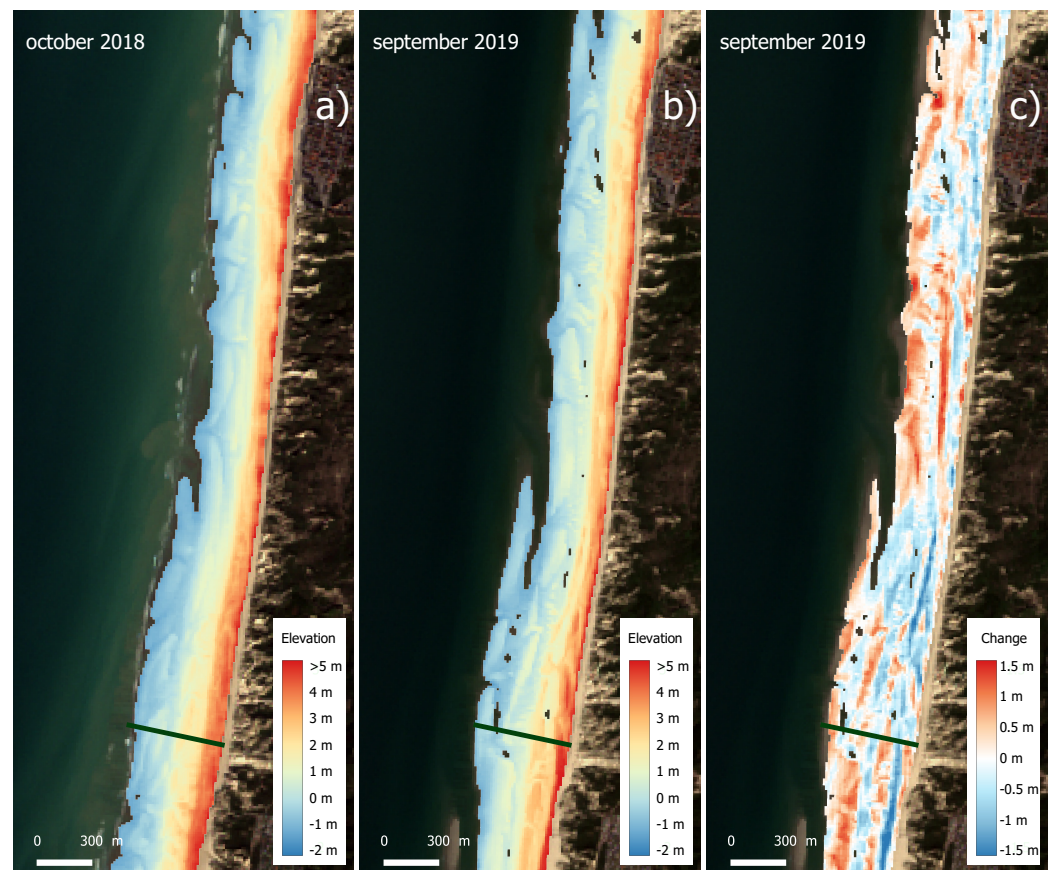
Figure 5. (**a**) DEM constructed from z_{model} of October 2018 and (**b**) of September 2019. (**c**) Elevation changes DEM from 2018 to 2019. Background: Sentinel-2 RGB composite imagery.

A first gridded DEM is constructed by triangular interpolation of these 8 water-lines (Figure 7a) and compared to the DEM of the February 2019 in situ measurements (Figure 7b). The agreement with the observed values is quantified by a coefficient R^2 equal to 0.945 and a height accuracy (rmse) of 0.355 m. The second DEM built from 7 water lines is also in good agreement with the measurement campaign of the October 2019 period (Figure 7c,d). The R^2 coefficient value of 0.941 and the height accuracy of 0.376 m attest to the robustness of the waterline method when applied to the Authie Bay. By construction, the waterlines DEM is limited in its edge by the high tide shoreline, whereas the obser-vational DEM can give information beyond this shoreline, as is the case for the Bec du Perroquet area (Figure 7b). The erosion of this eight-meter high dune line is clearly visible on these maps despite the short time period from February to October 2019 (Figure 7c).
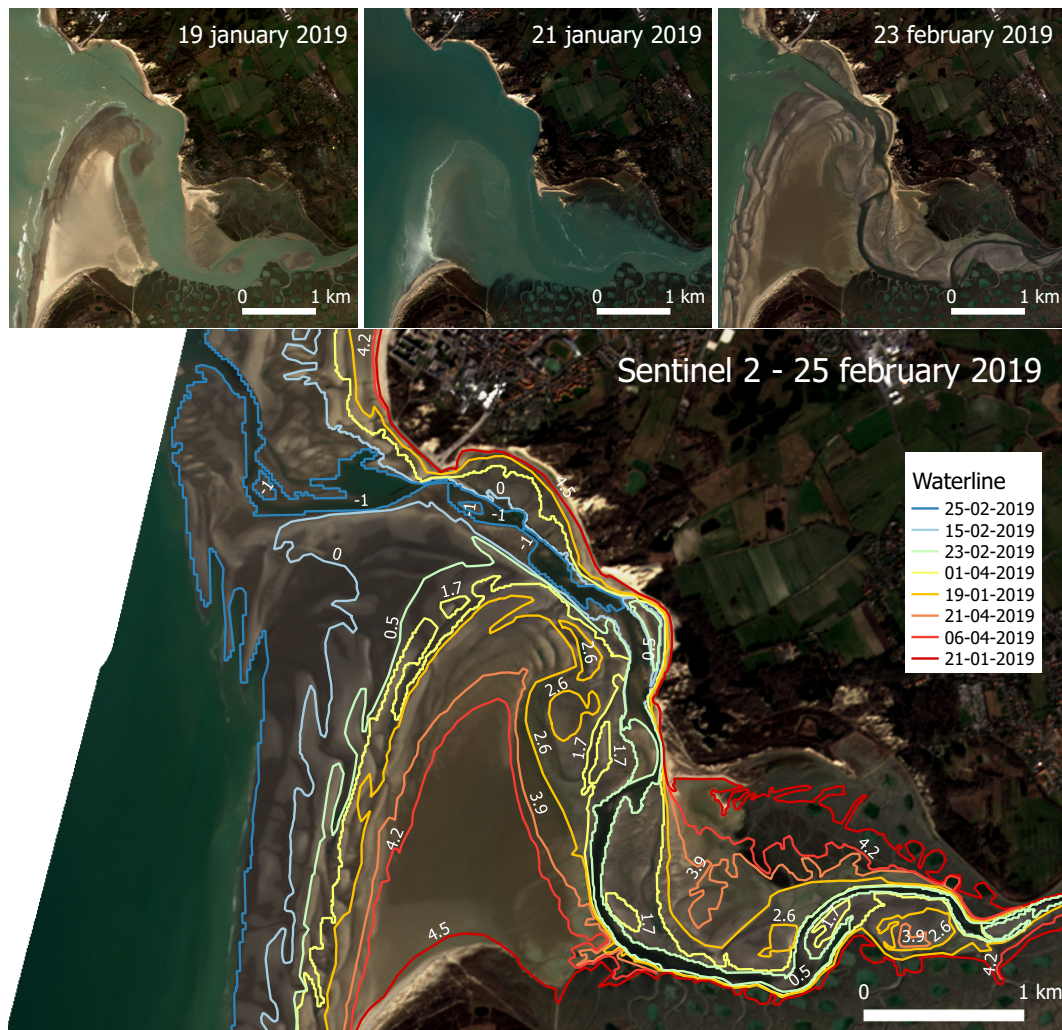
Figure 6. Sample of Sentinel-2 satellite images of various tides and waterlines extracted from these images. Labels refer to the height(m) assigned to each waterline.

Differentiation of the DEMs allows the mapping of the elevation changes over this period (Figure 8a). Downstream of the bay, variations in topography result from the migration of the littoral dunes from the south to the north of the shoreline, under the effect of the longshore drift, and then curving eastwards along the spit platform. Outside the observation area, this mapping allows the detection of high sedimentation at two locations upstream of the Bec du Perroquet area. To verify that this result is not an artifact of the modeling, two almost identical satellite images of intermediate low tide levels are compared. The waterline height on the Sentinel-2 image of 1 April 2019 is 1.70 m (Figure 8b), while that of 30 November is 2.10 m (Figure 8c). This 40 cm difference is visible west of the spit platform which appears slightly more submerged in November. Although the tide level is slightly higher in this image, two areas indicated by arrows appear emerged, thus confirming the sedimentation anomaly detected by the evolution mapping.
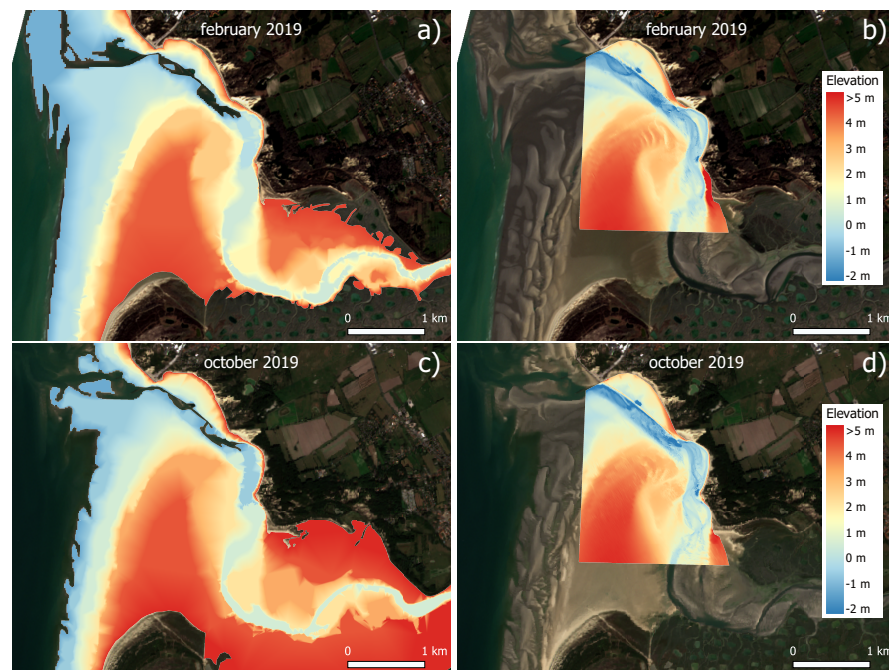
Figure 7. (**a**) DEM constructed using the waterline method, compared to observations (**b**) made in February 2019. (**c,d**) The same for the October 2019 period. Background: Sentinel-2 imagery.
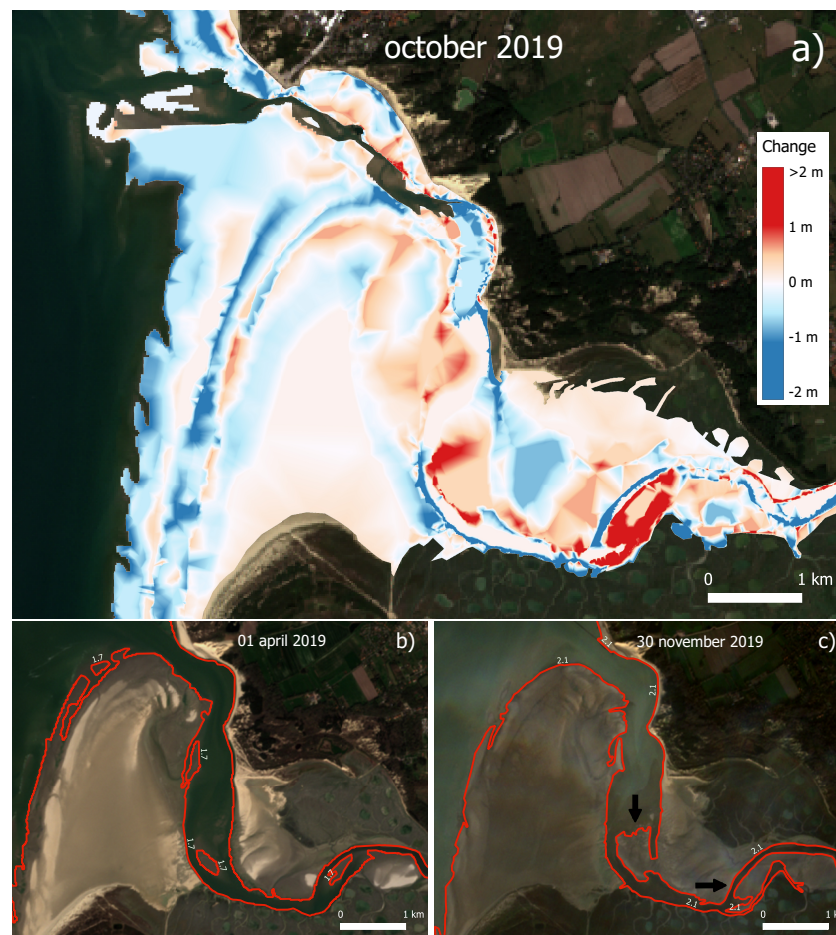

Figure 8. (**a**) Map of elevation changes from February to October 2019. (**b,c**) Sentinel-2 images of intermediate low tide with corresponding waterlines (red lines). Black arrows indicate areas experiencing a high sedimentation phase over the period April to November 2019.

3.2.2. Morphological Changes

Video animations of remote sensing images provide initial information on the morphological evolution of the area. The longshore drift generated by the longshore current is visible on timelapses of low tide images. The displacement of littoral dunes from south coast to north thus creates a sedimentary connection between the Somme, Authie and Canche bays. From the location of the sedimentary bars, the drift velocity is evaluated to 400 ± 50 m per year. The drift time scale is therefore 30 ± 5 years between the Somme and Authie bays, which are 12 kms apart and 40 ± 5 years for a distance of 16 kms between the Authie and Canche bays. At the estuarine mouth, the longshore transport curves along the spit platform that it supplies and collides with the Authie flow channel. Inward and outward sand currents emerge from the resulting shock front.

During high tides, the spit platform and salt marshes, shown in Figure 1b, are submerged. The corresponding satellite images allow the evolution of the coastline to be mapped (Figure 9).
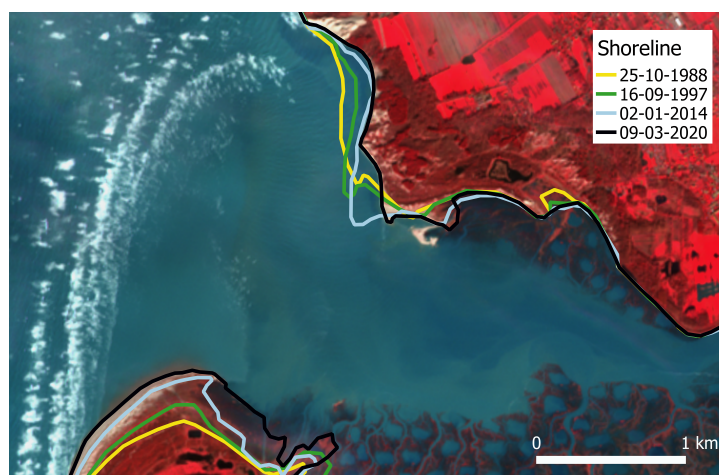

Figure 9. Shoreline evolution of the Authie Bay from 1988 to 2020. Background: Sentinel-2 false-color composite imagery.

The shoreline retreated steadily by 220 m in the area bordering Bois des Sapins from 1988 to 2020, i.e., a rate of 7 m per year. The situation is more complex in the Bec du Perroquet area, with first a sedimentation phase from 1988 to 1997 and then a strong erosion stage from 2014 to 2020, causing the coastline to recede by 190 m. On the contrary, by deposition of the sand brought back by the longshore drift, the base of the sandspit has progressed by 320 m over the period 1988 to 2020, i.e., at a rate of 10 m/yr.

The tidal basin corresponding to high tides does not provide information on the internal processes of the bay. More interesting are the intermediate tides for which the sand platform is emerged. Timelapses of intermediate tide images suggest that the Authie tidal basin can then decline into an upper and a lower tidal basin. The upper one is defined by a submerged upstream part of the bay and an emerged sandspit. As shown in Figure 10, this upper tidal basin changes little in the Bois des Sapins and Bec du Perroquet areas from 1985 to the present day (transects A and B). In contrast, the large decrease in size of the upper tidal basin upstream of the bay, between transects C and D, implies sediment deposition over this period, allowing the extension of the vegetation cover (Figure 10b). The lower tidal basin is defined by an upstream emerged part of the bay and an emerged sandspit (Figure 10c,d). Video animations show that prior to 2015, upper and lower basins merged between transects A and B. Since then, the width of the lower basin has been halved, implying a deposition of sediments to the east of the sandspit, thus constraining the flow channel to the eastern shore.

However, the detection of tidal basin boundaries from satellite images of intermediate tides is approximate due to the tidal range. It is therefore necessary to ensure that the apparent evolution of the lower tidal basin is not an artifact due to data from an unrepresentative sample. Of the collection of 413 satellite images, more than half are low or near low tide images. Between 1984 and 2014, the remaining images in the collection are distributed as follows: 18 meet the lower tidal basin criterion, 3 images are unclassified, 41 meet the upper tidal basin criterion, and 19 are high tide images (i.e., with a partially or fully submerged sand platform). The 18 images with a lower tidal basin resemble the one in Figure 10c. Of the images from 2015 to 2020, 32 meet the lower tidal basin criterion, 5 are unclassified, 46 meet the upper tidal basin criterion, and 29 are high tide images. The lower tidal basin for the sample of 32 images has a similar appearance to that in Figure 10d. The robustness of this qualitative approach attests to the existence of sedimentation at the east side of the spit platform.
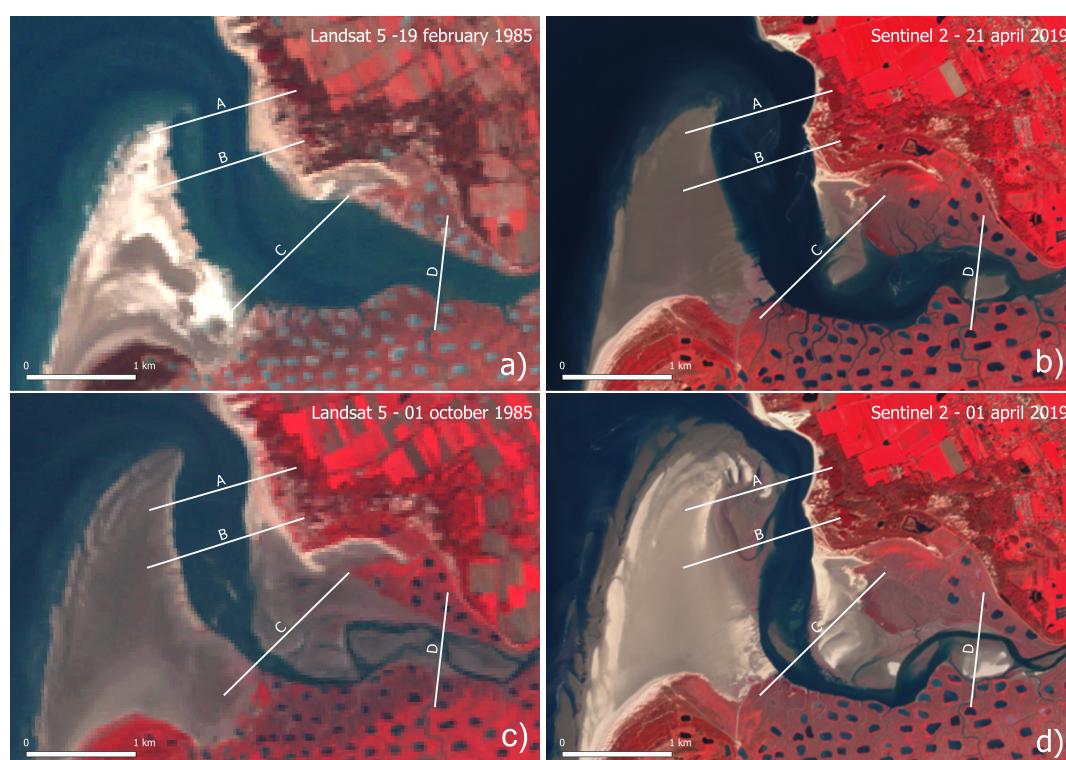

Figure 10. (**a**,**b**) Evolution of the upper Authie tidal basin from 1985 to 2019. The criterion for defining the upper basin is both the emerged spit platform and the submerged upstream bay. (**c**,**d**) Evolution of the lower Authie tidal basin from 1985 to 2019. The criterion for defining the lower basin is both the emerged spit platform and the emerged upstream bay. Chronicles of the minor river bed changes are recorded along transects A to D.

Chronicles of the Authie meanders for transect B are presented in Figure 11, to contextualize the erosion of the Bec du Perroquet area. Boundaries of the upper basin are indicated by green solid lines, and those of the lower basin, by dashed lines. The relative position of the main flow channel along transect B is marked by a dark blue line. A light blue dot indicates the position of a secondary channel if it exists. In most cases, the secondary channel is located in the opposite configuration to the main channel and represents an alternative flow solution. According to theses chronicles, the past timescale in a configuration is a few years, while the switchover timescale is a few months. The tidal basin boundaries, although imprecise, appear to be relatively stable and are shown only to visualize the spatial limits of the Authie channel wanderings. However, the eastern boundary of the upper tidal basin on transects A and B has very little dependence on tidal level due to the steepness of the dunes in this area and can be assimilated to the coastline.

From 1985 to 2015, the river wanderings had a spatial amplitude of one kilometer, i.e., the size of the lower tidal basin (Figure 11a). From 2015 onwards, the lower basin right-of-way was halved, forcing the Authie river to flow along the eastern bank (Figure 11b). From 2015 until early 2019, the erosion of the eastern bank rose up to a rate of 10 m/year and then accelerated sharply, causing the shoreline to retreat by 130 m in 2019 alone. A series of storms in spring 2020 reshaped the flow of the Authie river into a configuration opposite to the shore, putting an end to the intense erosion phase.
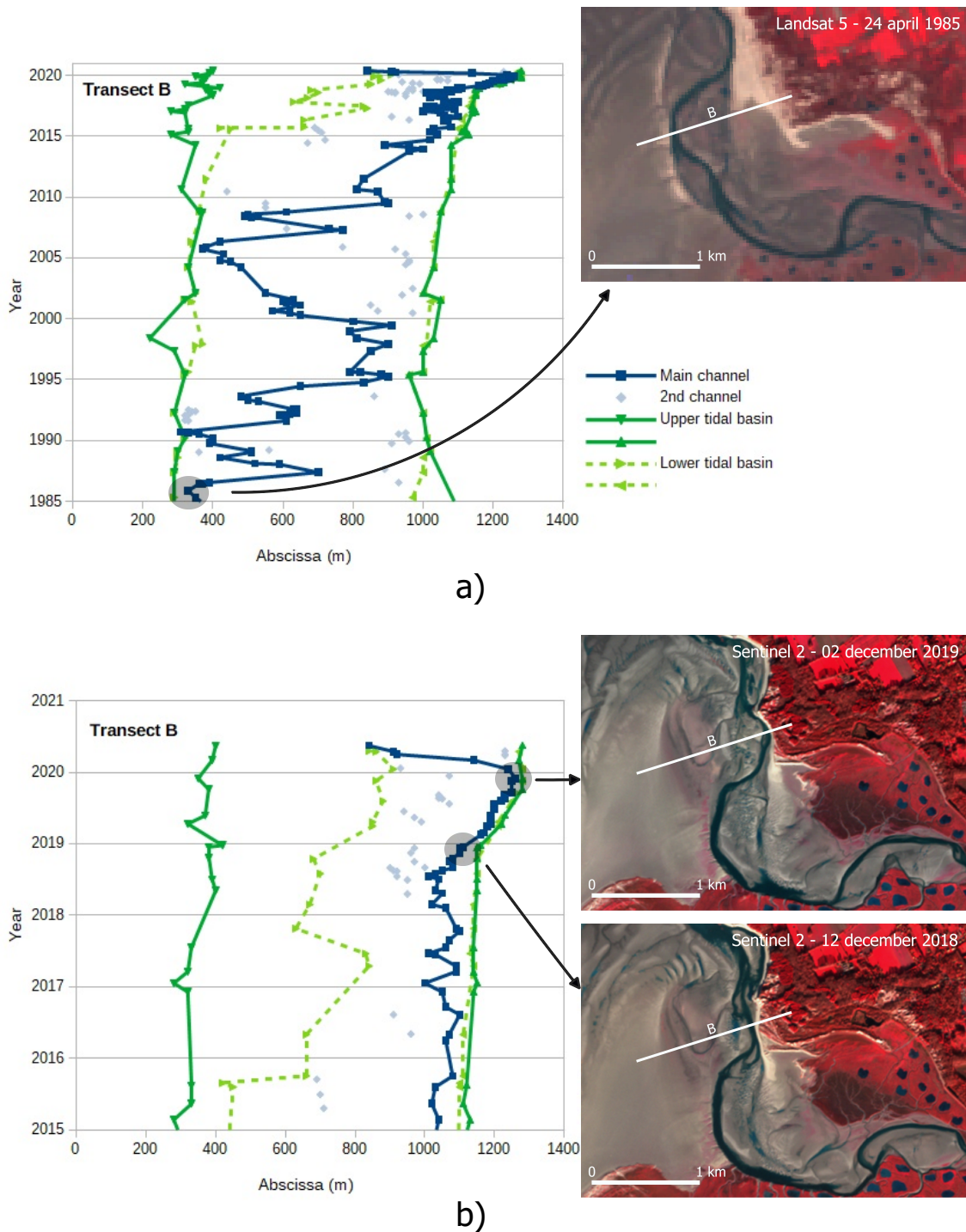

Figure 11. (**a**) Chronicles of the Authie meanders from 1985 to 2020 along transect B. (**b**) Zoom of the chronicles over the period 2015 to 2020.

According to the positions recorded on transect A (Figure 12), from 2015 onwards, the size of the lower tidal basin was reduced by two thirds, strongly restricting the Authie wanderings towards the eastern bank. From 1985 to 2020, the retreat of the eastern bank on the edge of the Bois des Sapins (transect A) is 270 m, i.e., an average erosion rate of 7.5 m per year, consistent with the erosion rate of 7 m/yr found from the shoreline evolution map in this area. Further upstream along the bay, the evolution of the flow channel on transect C is conditioned by the significant variations of the upper and lower tidal basins to the south-east of the Bec du Perroquet area. In particular, this area shows signs of a sedimentation phase since 2015 with a narrowing of these basins, pushing the Authie river towards the spit platform. Upstream of the bay, on transect D, the main channel shows typical tippings between two flow configurations on opposite edges. The secondary channel in the opposite configuration remains an alternative flow solution.
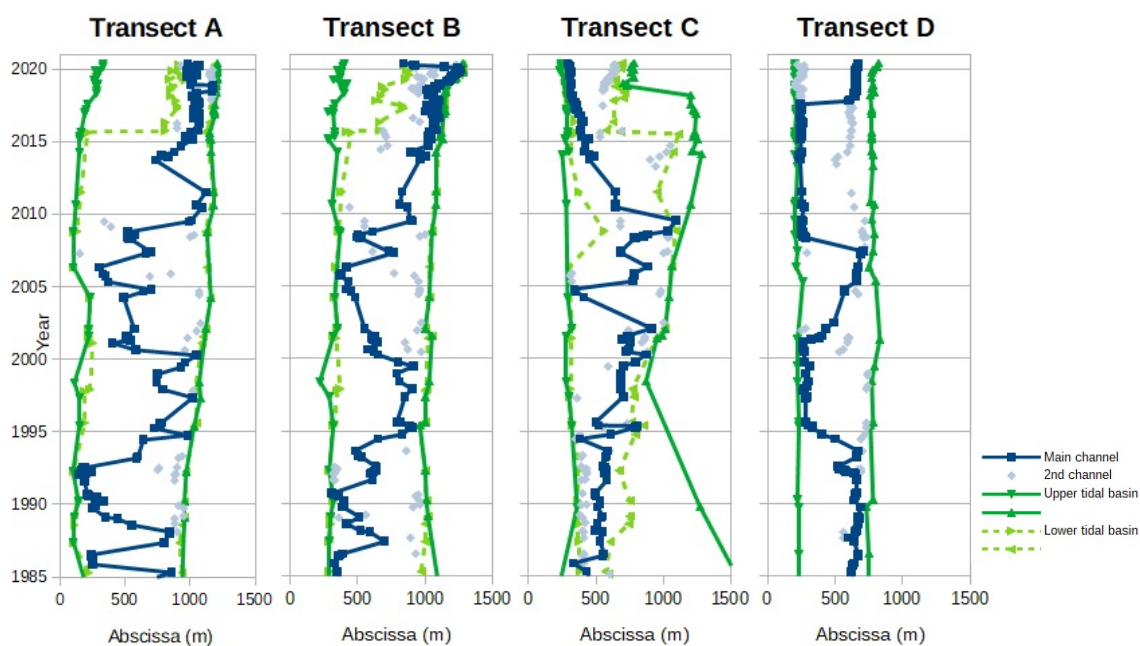

Figure 12. Chronicles of the Authie meanders from 1985 to 2020 along transects A to D.

4. Discussion

4.1. Relevance of Satellite-Derived Topography Models

The selection within the wide range of existing remote sensing techniques needs to consider the objective sought, the technical constraints of data acquisition for the study area, the repeatability of the procedure, the data processing time and the accuracy of the mapping resulting from the entire processing chain. SDB is a widely used method for mapping the nearshore zone, based on detection of light reflected from the seafloor. Whether from empirical methods requiring calibration with in situ data or from semi-analytical algorithms using radiative transfer models, many recent studies have shown the value of SDB for shallow waters with good transparency conditions (e.g., [31,32] and the review [7]). However, depth retrieval is limited by water turbidity in dynamic areas such as tidal inlets [33]. Sanchez et al. (2014) [34] highlighted the influence of turbidity on the accuracy of results obtained from empirical methods. Height accuracy better than 0.5 m was found in low turbidity environments with depths ranging from 0 to 6 m, while accuracy dropped to 0.9 m in the turbid waters of a mesotidal estuary mouth. In the preparatory work for this study, we carried out some tests of the SDB method and found that the reflectance of the optical bands correlated poorly with the in situ depth measurements, which confirmed the apparent turbidity in the remote sensing images. The height accuracy obtained by the SDT models (Table 3) is probably better than that to be expected from a

SDB method in this rapidly changing and very turbid environment. The inherent limitation of SDT is its restriction to the intertidal zone whereas SDB allows for extensive mapping in the nearshore zone. However, the maximum tidal range of 8.5 m in the Authie Bay partially eliminates this drawback by allowing most of the bay to be mapped by a SDT method.

Table 3. Accuracy assessment of satellite-derived topography models.

Assessment	Berck Shoreline		Authie Bay	
	October 2018	September 2019	February 2019	October 2019
R^2	0.950	0.965	0.945	0.941
rmse (m)	0.345	0.300	0.355	0.376

The SDT method developed for the Berck shoreline site is based on the statistical relationship between variations in the green band reflectance of a low-tide image and those of the topography. We assumed that a topographic signal of the intertidal zone can be described as a combination of two signals, one slowly varying in space, which can be related to the natural slope of the beach, and the other rapidly varying signal carrying the spatial information of small sedimentary structures such as sedimentary bars. It was shown, by the good agreement between the DEM model and in situ measurements (Table 3), that this rapidly varying signal was well represented by the green band reflectance. This dependence is simply explained by the decrease in reflectance with increasing moisture content. Variations in scattering and absorption of light are attributed to the interstitial water surrounding the sand grains [35]. Thus, on a low tide image, the wet sand on the slopes or between coastal dunes appears darker than the dry sand layer on the dune crest. The moisture content therefore depends roughly on the dune morphology but also on the time spent out of the water, i.e., on its relative position on the intertidal zone. Recently Kang et al. (2020) [16] developed an artificial neural network to simulate the topography of fast-changing tidal flats. The training data from remote sensing images, as the input layer of their neural network, were the geographical coordinates, the distance from the waterlines and multi spectral bands that were considered as elevation-related elements. This approach allowed to construct DEMs with a height accuracy of 0.3 to 0.4 m compared to in situ measurements. Thus, the interest of remote sensing spectral bands for the intertidal zone, as a relevant source of topographic information, is highlighted through the approach of Kang et al., as well as the SDT model proposed here for the Berck shoreline site.

The SDT model of the Authie Bay relies exclusively on the waterline method. Remote sensing images were selected over a time interval of one season centered on the date of acquisition of the in situ measurements so that the morphological changes were not too significant. The manually digitized waterlines were then assembled to construct DEMs, which proved to be in good agreement with the observations with a height accuracy of 35 to 38 cm. Recent studies based on the waterline method commonly reported height accuracies ranging from 10 to 40 cm [28,36–39]. The accuracy of the resulting DEM depends mainly on the well-distributed sampling of the tidal range, which implies a large variety of waterlines. In previous studies, the time interval of the extracted waterlines spans one or more years, which does not hinder in the case of slowly changing environments nor when studying topographic changes over a period much longer than the acquisition period [15]. However, for rapidly varying environments, the characteristic time scale is necessarily smaller: three months for the SDT model monitoring the Authie Bay and only one month for the rapidly changing tidal flats of the Jiangsu coast in China [16]. The height accuracy of the Authie Bay model may be improved by incorporating SAR satellite images in addition to those from Sentinel-2, and by further exploring the inclusion of spectral reflectance in the SDT model, motivated by the results from the Berck shoreline site.

4.2. Interpretation of Morphological Changes

The Authie Bay is a macrotidal estuarine system, part of a group of three close estuaries on the north coast of France. Video animations showed a sedimentary connection from

south to north, between the Somme, Authie and Canche bays, resulting from the longshore drift. This wave-driven longshore transport of sediment feeds the spit platform of the Authie Bay and continues upstream of the estuary, visible as sand currents in the timelapses of low tide images. This visual observation seems to be in line with the current model of tide-dominated estuarine systems which show a trend to sedimentary infilling [3]. It is interpreted as a consequence of non-linear effects acting on the propagation of the ocean tidal wave, which become important in the case of strong tidal range in shallow environments. When the crest of the flood wave moves faster in deep water than the trough of the ebb tide, an asymmetry appears on the tidal wave, resulting in a shorter flood duration and a longer ebb duration. As a result, flood currents are stronger than ebb currents and carry more sand since the sediment load carried increases with the current velocity. Thus, flood dominant tidal asymmetry leads to a net import of marine sediment, for estuarine systems with small river inflow like the Authie bay.

The tide propagation inside the estuaries of the northern coast of France has the characteristics of a significant tidal asymmetry with a longer fall and a shorter rise. Anthony and Dobroniak (2000) [24] showed that the Authie Bay was in advanced state of infill, pointing out a large scale accretion of the estuary. Deloffre et al. (2007) [20] performed measurements of the sedimentation rhythms on the Authie mudflat and concluded that there is a correspondence with the semi-lunar cycle. They found a good correlation between tidal range and deposit thickness, which is consistent with the flood-dominant tidal currents model. Using Lidar data, Crapoulet et al. (2015) [40] quantified a positive net sediment budget for the overall Authie estuary between 2008 and 2011 and a negative net budget for the period 2011–2013. This trend of a negative net sediment budget for the whole estuary was confirmed by Verpooter et al. (2018) [26] for the period 2013–2016. However, they noted that the middle estuary, the back of the spit platform, experienced a positive rise. In the present study, it has been pointed out that the tidal basin of the middle estuary has split into an upper and a lower tidal basin from 2015 onwards, indicating that a sedimentation phase has occurred behind the spit platform. Pethick (1994) [41] described the main phases of estuary development on the basis of the estuarine channels types I and II defined by Dronkers (1986) [42]. The flood tide dominance of type I estuaries, with a wide and deep channel of rectangular cross-section, results in a positive net sediment budget. The continued intertidal deposition leads to a central channel type II bounded by high intertidal banks. An ebb dominance is then established, and these estuaries tend to become sediment exporters. The estuarine system then oscillates around a steady state position over a long period, alternating between type I and type II estuaries. The formation of the lower tidal basin in the Authie Bay could thus be the mark of a transition from type I to type II estuary, as described in the Pethick's model. Global sea level rise is expected to impact equilibrium morphology. In small, shallow estuaries, such as Authie Bay, an increase in water depth would result in a reduction in friction, which would lead to an amplification of the tide, thus enhancing the risk of flooding at high tide [5].

Chronicles of the Authie meanders showed that, in response to sedimentation on the sheltered side of the spit platform, the flow channel has been pushed towards the thick dune fields along the north-eastern shore since the 2010s and significantly since 2015 with the formation of the lower tidal basin. As a result, the north-eastern shoreline has undergone massive erosion in the areas of Bois des Sapins and Bec du Perroquet, leading to the weakening of the dune ridge that protects low-lying zones. This erosion pattern reached its peak in 2019, the year of an intense erosion phase in the Bec du Perroquet area, where a shoreline recession of 130 m in the space of a few months was recorded along a transect. Figure 11b shows that this erosion phase is regular throughout this year and does not appear to be induced by any particular storm event. At the end of 2018, the Authie river flows along the sand platform and then turns toward the Bec du Perroquet bank where it forms a sharp bend, a configuration that could explain the beginning of the erosion phase. Thus, a higher flow velocity at the outer bend erodes the bank further and could account for the shoreline recession in this area, as suggested in Figure 13. In 2020, following

a series of storms, the Authie resumes a straight flow along the sand platform ending the erosion phase, which seems to be in agreement with this hypothesis. Analysis of aerial photographs of the last decades [24] has shown that sand eroded from the northeast shore is temporarily stored on the beach and then transported up the bay and recycled into sandy-muddy intertidal flats or feeds the southward prograding of the Bec du Perroquet area [21]. These past observations suggest that the sedimentation anomaly upstream of the bay, revealed by the evolutionary mapping between February and October 2019, actually originated from the erosion 2019 event that affected the dunes in the Bec du Perroquet area.
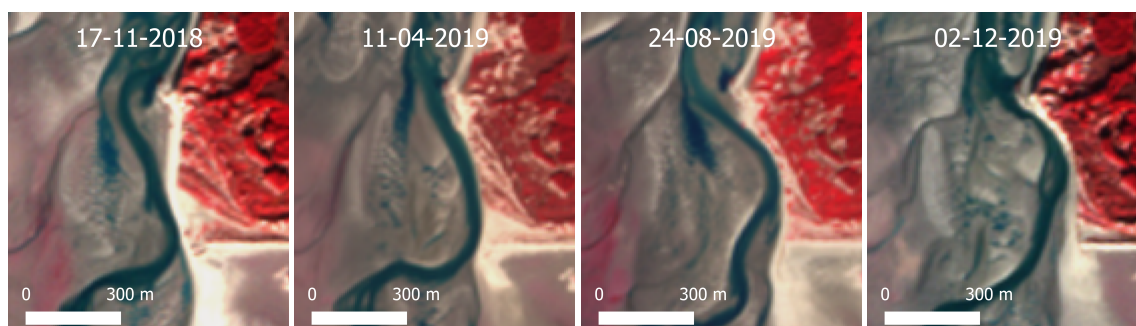

Figure 13. Sentinel-2 images of the Bec du Perroquet area during the 2019 erosion phase. Bank erosion is occurring primarily on the outer bend of the meander.

5. Conclusions

Satellite-derived bathymetry is known to be very effective in retrieving water depths in the nearshore zone but is hampered by turbidity in fast moving areas, such as estuarine systems, where it loses accuracy. This difficulty in mapping the seabed can be overcome in environments with large tidal ranges, by performing instead satellite-derived topography based on the waterline method. In this paper, this technique applied to the Authie macrotidal estuary allowed the construction of DEMs with a height accuracy better than 0.40 m. On the surrounding coast, simpler to map, a topography technique was developed, based on the green band reflectance of Sentinel-2 images, and enabled the discrimination of sandbars with a height accuracy of 0.30 to 0.35 m. These results confirm the value of satellite-derived topography in macrotidal environments.

Satellite imagery also has a temporal dimension and provides information on the major trends in the bay dynamics. Thus, from a collection of Landsat and Sentinel-2 satellite images from 1984 to 2020, a sedimentary connection between the Somme, Authie and Canche bays is highlighted, a history of the Authie meanders is retraced and change of the shoreline is mapped. In particular, a mean erosion rate of 7.5 m/year is evaluated for the Bois des sapins vulnerable area over this period. From 2015 onwards, the evolution of the tidal basin back to the spit platform has been indicative of high sedimentation in the middle estuary. In this self-organizing system, the erosion of the north-eastern shoreline within the Authie Bay appears to be a morphodynamic adjustment response to the constraint exerted on the Authie flow channel. Up to now, it is not straightforward to identify the main factor causing the channel migration. It is thus planned to build a numerical model to better analyze the influence of the different external forces (tide, flowrate and waves) on the local circulation and associated residual fluxes. The satellite derived topographic data will serve to validate the numerical morphodynamic model. The erosion pattern culminated in the intense erosion phase of 2019, which resulted in a 130 m retreat of the shoreline in the Bec du Perroquet area. Differentiation of DEMs constructed from satellite-derived topography revealed a sedimentation anomaly upstream of the bay that is interpreted as being related to the 2019 event.

Author Contributions: Conceptualization, P.B.; methodology, P.B.; validation, P.B.; formal analysis, P.B.; resources, P.B. and N.H.; writing–original draft, P.B. and N.H.; writing–review and editing, P.B., N.H. and P.S.; visualization, P.B.; supervision, N.H. and P.S.; project administration, N.H. and P.S.;

Abbreviations

The following abbreviations are used in this manuscript:

DEM	Digital Elevation Model
SDB	Satellite Derived Bathymetry
SDT	Satellite Derived Topography

References

1. Green, M.; Macdonald, I. Processes driving estuary infilling by marine sands on an embayed coast. *Mar. Geol.* **2001**, *178*. [CrossRef]
2. Tessier, B.; Billeaud, I.; Sorrel, P.; Delsinne, N.; Lesueur, P. Infilling stratigraphy of macrotidal tide-dominated estuaries. Controlling mechanisms: Sea-level fluctuations, bedrock morphology, sediment supply and climate changes (The examples of the Seine estuary and the Mont-Saint-Michel Bay, English Channel, NW France). *Sediment. Geol.* **2012**, *279*, 62–73. [CrossRef]
3. Dronkers, J. *Dynamics of Coastal Systems*, 2nd ed.; World Scientific: Singapore, 2016. [CrossRef]
4. Michel, C.; Bot, S.L.; Druine, F.; Costa, S.; Levoy, F.; Dubrulle-Brunaud, C.; Lafite, R. Stages of sedimentary infilling in a hypertidal bay using a combination of sedimentological, morphological and dynamic criteria (Bay of Somme, France). *J. Maps* **2017**, *13*, 858–865. [CrossRef]
5. Leuven, J.; Pierik, H.J.; van der Vegt, M.; Bouma, T.; Kleinhans, M. Sea-level-rise-induced threats depend on the size of tide-influenced estuaries worldwide. *Nat. Clim. Chang.* **2019**, *9*, 986–992. [CrossRef]
6. Mason, D.; Gurney, C.; Kennett, M. Beach topography mapping—A comparison of techniques. *J. Coast. Conserv.* **2000**, *6*, 113–124. [CrossRef]
7. Salameh, E.; Frappart, F.; Almar, R.; Baptista, P.; Heygster, G.; Lubac, B.; Raucoules, D.; Almeida, L.P.; Bergsma, E.W.J.; Capo, S.; et al. Monitoring Beach Topography and Nearshore Bathymetry Using Spaceborne Remote Sensing: A Review. *Remote Sens.* **2019**, *11*, 2212. [CrossRef]
8. Lyzenga, D.R. Passive remote sensing techniques for mapping water depth and bottom features. *Appl. Opt.* **1978**, *17*, 379–383. [CrossRef]
9. Lyzenga, D.R. Shallow-water bathymetry using combined lidar and passive multispectral scanner data. *Int. J. Remote Sens.* **1985**, *6*, 115–125. [CrossRef]
10. Gao, J. Bathymetric mapping by means of remote sensing: Methods, accuracy and limitations. *Prog. Phys. Geogr. Earth Environ.* **2009**, *33*, 103–116. [CrossRef]
11. Caballero, I.; Stumpf, R.; Meredith, A. Preliminary Assessment of Turbidity and Chlorophyll Impact on Bathymetry Derived from Sentinel-2A and Sentinel-3A Satellites in South Florida. *Remote Sens.* **2019**, *11*, 645. [CrossRef]
12. Caballero, I.; Stumpf, R.P. Towards Routine Mapping of Shallow Bathymetry in Environments with Variable Turbidity: Contribution of Sentinel-2A/B Satellites Mission. *Remote Sens.* **2020**, *12*, 451. [CrossRef]
13. Mason, D.C.; Davenport, I.J.; Robinson, G.J.; Flather, R.A.; McCartney, B.S. Construction of an inter-tidal digital elevation model by the 'Water-Line' Method. *Geophys. Res. Lett.* **1995**, *22*, 3187–3190. [CrossRef]
14. Mason, D.C.; Davenport, I.J.; Flather, R. Interpolation of an intertidal digital elevation model from heighted shorelines: A case study in the Western Wash. *Estuar. Coast. Shelf Sci.* **1997**, *45*, 599–612. [CrossRef]

15. Li, Z.; Heygster, G.; Notholt, J. Intertidal Topographic Maps and Morphological Changes in the German Wadden Sea between 1996–1999 and 2006–2009 from the Waterline Method and SAR Images. *IEEE J. Sel. Top. Appl. Earth Obs. Remote Sens.* **2014**, *7*, 3210–3224. [CrossRef]

16. Kang, Y.; Lv, W.; He, J.; Ding, X. Remote Sensing of Time-Varying Tidal Flat Topography, Jiangsu Coast, China, Based on the Waterline Method and an Artificial Neural Network Model. *Appl. Sci.* **2020**, *10*, 3645. [CrossRef]

17. Cham, D.; Son, N.; Nguyen, M.; Tien Thanh, N.; Dung, T. An Analysis of Shoreline Changes Using Combined Multitemporal Remote Sensing and Digital Evaluation Model. *Civ. Eng. J.* **2020**, *6*, 1–10. [CrossRef]

18. Nazeer, M.; Waqas, M.; Shahzad, M.I.; Zia, I.; Wu, W. Coastline Vulnerability Assessment through Landsat and Cubesats in a Coastal Mega City. *Remote Sens.* **2020**, *12*, 749. [CrossRef]

19. Capo, S.; Lubac, B.; Marieu, V.; Robinet, A.; Bru, D.; Bonneton, P. Assessment of the decadal morphodynamic evolution of a mixed energy inlet using ocean color remote sensing. *Ocean Dyn.* **2014**, *64*, 1517–1530. [CrossRef]

20. Deloffre, J.; Verney, R.; Lafite, R.; Lesueur, P.; Lesourd, S.; Cundy, A. Sedimentation on intertidal mudflats of macrotidal estuaries: Sedimentation, rhythms and their preservation. *Mar. Geol.* **2007**, *241*, 19–32. [CrossRef]

21. Hesp, P.; Ruz, M.H.; Hequette, A.; Marin, D.; da Silva, G.M. Geomorphology and dynamics of a traveling cuspate foreland, Authie estuary, France. *Geomorphology* **2015**, *254*, 104–120. [CrossRef]

22. Marion, C.; Anthony, E.; Alain, T. Short-term (<2 yrs) estuarine mudflat and saltmarsh sedimentation: High-resolution data from ultrasonic altimetery, rod surface-elevation table, and filter traps. *Estuar. Coast. Shelf Sci.* **2009**, *83*, 475–484. [CrossRef]

23. Dobroniak, C.; Anthony, E. Short-term Morphological Expression of Dune Sand Recycling on a Macrotidal, Wave-Exposed Estuarine Shoreline. *J. Coast. Res.* **2002**, *36*, 240–248. [CrossRef]

24. Anthony, E.; Dobroniak, C. Erosion and recycling of aeolian dunes in a rapidly infilling macrotidal estuary: The Authie, Picardy, northern France. *Geol. Soc. Lond. Spec. Publ.* **2000**, *175*, 109–121. [CrossRef]

25. Dobroniak, C. Morphological evolution and management proposals in the Authie Estuary, northern France. *Proc. Dunes Estuaries* **2005**, *2205*, 537–545.

26. Verpoorter, C.; Menuge, B.; Launeau, P.; Méléder, V.; Héquette, A.; Cartier, A.; Sipka, V. *Synergy between Hyperspectral (HYSPEX), Multispectral (SPOT 6/7, Sentinel-2) Remotely Sensed Data and LiDAR Data for Mapping the Authie Estuary (France)*. *Estuaries and Coastal Zones in Times of Global Change*; Nguyen, K.D., Guillou, S., Gourbesville, P., Thiébot, J., Eds.; Springer: Singapore, 2020; pp. 769–788.

27. Sentinel Hub EO Browser. Available online: https://apps.sentinel-hub.com/eo-browser (accessed on 30 March 2021).

28. Mason, D.; Scott, T.; Dance, S. Remote sensing of intertidal morphological change in Morecambe Bay, U.K., between 1991 and 2007. *Estuar. Coast. Shelf Sci.* **2010**, *87*, 487–496. [CrossRef]

29. Kang, Y.; Ding, X.; Xu, F.; Zhang, C.; Ge, X. Topographic mapping on large-scale tidal flats with an iterative approach on the waterline method. *Estuar. Coast. Shelf Sci.* **2017**, *190*, 11–22. [CrossRef]

30. Xu, Z.; Kim, D.-j.; Kim, S.H.; Cho, Y.K.; Lee, S.G. Estimation of seasonal topographic variation in tidal flats using waterline method: A case study in Gomso and Hampyeong Bay, South Korea. *Estuar. Coast. Shelf Sci.* **2016**, *183*, 213–220. [CrossRef]

31. Eugenio-Gonzalez, F.; Marcello, J.; Abasolo, J.M. High-Resolution Maps of Bathymetry and Benthic Habitats in Shallow-Water Environments Using Multispectral Remote Sensing Imagery. *IEEE Trans. Geosci. Remote Sens.* **2015**, *53*, 3539–3549. [CrossRef]

32. Evagorou, E.; Mettas, C.; Agapiou, A.; Themistocleous, K.; Hadjimitsis, D. Bathymetric maps from multi-temporal analysis of Sentinel-2 data: The case study of Limassol, Cyprus. *Adv. Geosci.* **2019**, *45*, 397–407. [CrossRef]

33. Pacheco, A.; Horta, J.; Loureiro, C.; Ferreira, Ó. Retrieval of nearshore bathymetry from Landsat 8 images: A tool for coastal monitoring in shallow waters. *Remote Sens. Environ.* **2015**, *159*, 102–116. [CrossRef]

34. Sánchez-Carnero, N.; Ojeda-Zujar, J.; Rodríguez-Pérez, D.; Marquez-Perez, J. Assessment of different models for bathymetry calculation using SPOT multispectral images in a high-turbidity area: The mouth of the Guadiana Estuary. *Int. J. Remote Sens.* **2014**, *35*, 493–514. [CrossRef]

35. Nolet, C.; Poortinga, A.; Roosjen, P.; Bartholomeus, H.; Ruessink, G. Measuring and Modeling the Effect of Surface Moisture on the Spectral Reflectance of Coastal Beach Sand. *PLoS ONE* **2014**, *9*, e112151. [CrossRef] [PubMed]

36. Ryu, J.H.; Kim, C.; Lee, Y.K.; Won, J.S.; Chun, S.S.; Lee, S. Detecting the intertidal morphologic change using satellite data. *Estuar. Coast. Shelf Sci.* **2008**, *78*, 623–632. [CrossRef]

37. Zhao, B.; Guo, H.; Yan, Y.; Wang, Q.; Li, B. A simple waterline approach for tidelands using multi-temporal satellite images: A case study in the Yangtze Delta. *Estuar. Coast. Shelf Sci.* **2008**, *77*, 134–142. [CrossRef]

38. Liu, Y.; Li, M.; Cheng, L.; Li, F.; Chen, K. Topographic Mapping of Offshore Sandbank Tidal Flats Using the Waterline Detection Method: A Case Study on the Dongsha Sandbank of Jiangsu Radial Tidal Sand Ridges, China. *Mar. Geod.* **2012**, *35*, 362–378. [CrossRef]

39. Tong, S.S.; Deroin, J.P.; Pham Thi, L. An optimal waterline approach for studying tidal flat morphological changes using remote sensing data: A case of the northern coast of Vietnam. *Estuar. Coast. Shelf Sci.* **2020**, *236*, 106613. [CrossRef]

40. Crapoulet, A. Evolution du trait de côte, Bilans Sédimentaires et Évaluation des Zones à Risques sur le Littoral du Nord-Pas-de-Calais: Analyse Multi-échelles par LiDAR aéroporté. Ph.D. Thesis, Université du Littoral Côte d'Opale, Villeneuve d'Ascq, France, 2015.

41. Pethick, J. *Estuaries and Wetlands: Function and Form*; Thomas Telford Publishing: London, UK, 1994; pp. 75–87. [CrossRef]

42. Dronkers, J. Tidal asymmetry and estuarine morphology. *Neth. J. Sea Res.* **1986**, *20*, 117–131. [CrossRef]